

# Exploring Systematic Discrepancies in DFT Calculations of Chlorine Nuclear Quadrupole Couplings

*Ondřej Socha,<sup>a</sup> Paul Hodgkinson,<sup>b</sup> Cory M. Widdifield,<sup>b</sup> Jonathan R. Yates<sup>c</sup> and Martin  
Dračínský<sup>\*a</sup>*

<sup>a</sup>Institute of Organic Chemistry and Biochemistry, Flemingovo nám. 2, 16610, Prague, Czech  
Republic

<sup>b</sup>Department of Chemistry, Durham University, South Road, DH1 3LE, Durham, UK

<sup>c</sup>Department of Materials, University of Oxford, Parks Road, Oxford OX1 3PH, UK

ABSTRACT: Previous studies revealed significant discrepancies between DFT-calculated and experimental nuclear quadrupolar coupling constants ( $C_Q$ ) at chlorine atoms, particularly in ionic solids. Various aspects of the computations are systematically investigated here, including the choice of the DFT functional, basis set convergence, and geometry optimization protocol. The effect of fast (fs) time-scale dynamics are probed using molecular dynamics (MD) and nuclear quantum effects (NQEs) are considered using path-integral MD calculations. It is shown that the functional choice is the most important factor related to improving the accuracy of the

quadrupolar coupling calculations and functionals beyond the generalized gradient approximation (GGA) level, such as hybrid and meta-GGA functionals, are required for good correlations with experiment. The influence of molecular dynamics and NQEs is less important than the functional choice in the studied systems. A method which involves scaling the calculated quadrupolar coupling constant is proposed here; its application leads to good agreement with experimental data.

## **Introduction**

Chlorine-containing systems are regularly found in various areas of chemistry, biology and material science. Many chlorine-containing compounds have been isolated from organisms ranging from prokaryotes to mammals,<sup>1-2</sup> and chloride ions are the most abundant negative ions in every living cell.<sup>3</sup> Chlorine is also exceptionally important in industry.<sup>4</sup> For example, it has been estimated that 15000 organochlorine compounds are used commercially.<sup>5</sup> Further, 88 % of the top selling pharmaceuticals in 2012 used chlorine chemistry at some stage in their manufacture,<sup>6</sup> and hydrochlorides of active pharmaceutical ingredients (APIs) comprised ca 15 % of solid pharmaceuticals.<sup>7-8</sup> Chlorine atoms are also present in many minerals, glasses and catalysts, and chlorine is important from a crystal engineering perspective as it can form halogen bonds.<sup>9</sup>

Two conventional methods for the structural characterisation of solids are X-ray diffraction (XRD) and solid-state NMR (SS-NMR) spectroscopy. For XRD methods to be of use, they typically require a highly ordered crystalline sample and are inherently limited in the structural characterization of amorphous samples. As an alternative to XRD, SS-NMR spectroscopy is regularly applied to obtain atomic-level insights into the structure and dynamics of solids. For

example,  $^{13}\text{C}$  SS-NMR is commonly used as a structural probe of polymorphs in crystalline solids.<sup>10-11</sup>

Chlorine has two magnetically active and stable isotopes –  $^{35}\text{Cl}$  and  $^{37}\text{Cl}$ . The nuclei of both isotopes possess low gyromagnetic ratios and moderate nuclear electric quadrupole moments.<sup>12</sup> For nuclei which possess non-zero quadrupole moments, in addition to chemical shielding and spin–spin interactions, there exists an interaction between the quadrupole moment and the electric field gradient (EFG) at the nucleus. This interaction originates from the surrounding distribution of electrons and nuclei, and is described by the quadrupolar coupling constant ( $C_Q$ ) and asymmetry ( $\eta_Q$ ) parameters. The quadrupolar interaction is often larger than chemical shielding and spin-spin interactions, making SS-NMR studies of quadrupolar nuclides challenging for powdered samples due to lineshape broadening. However, recent advances in NMR instrumentation and methodology (high-field magnets, ultra-fast magic angle spinning,<sup>13-14</sup> double rotation,<sup>15-16</sup> dynamic angle spinning,<sup>17</sup> and multi-quantum magic angle spinning<sup>18</sup>) have made it possible to reduce the second-order quadrupolar broadening, and hence the acquisition of high-quality chlorine SS-NMR spectra is becoming more practical. In general, the quadrupolar interaction for ionic chloride-containing systems is much lower than for the covalent chlorine systems, and thus  $^{35/37}\text{Cl}$  SS-NMR spectroscopy has been an increasingly popular method for studying the environments of chloride ions in a variety of organic and inorganic materials over the past two decades.<sup>19-22</sup> However, it has recently been demonstrated that it is possible to acquire high-quality chlorine NMR spectra of compounds with covalently bound chlorine with relatively much larger  $C_Q$  values.<sup>23</sup> Both the EFG and chemical shielding tensors are sensitive reporters on the local molecular and electronic structure, and as such  $^{35/37}\text{Cl}$  SSNMR is a valuable tool for the characterization of chlorine containing compounds.<sup>24</sup> It has been shown, for

example, that chlorine EFG parameters can be correlated to the hydrogen-bonding environment.<sup>25</sup>

Chlorine SS-NMR can be used as a structural probe for many materials. For example, it has been used as a technique for polymorph distinction and in the screening of hydrochloride (HCl)-containing APIs<sup>25-28</sup> as well as their dosage forms with excipients, which is difficult for other techniques.<sup>29-30</sup> Chlorine SS-NMR has also been used for the characterization of a chloride ion receptor,<sup>21</sup> alkaline earth chlorides (including hydrates)<sup>24, 31</sup> and has been used to comment on halogen bonding<sup>32-34</sup> and ion dynamics in solids.<sup>35-36</sup> Chlorine SS-NMR has also found applications in the study of materials such as sodalities<sup>37</sup> and glasses.<sup>38</sup>

Computational studies often serve as a useful complement to SS-NMR experiments, providing additional information and aiding analysis, as quantum chemical calculations provide a direct link between structure and NMR observables. Several modelling and simulation techniques have been proposed to describe the influence of intermolecular interactions in solids on NMR parameters. In cluster models, neighboring molecules or fragments are considered explicitly during the NMR calculations. This cluster approach has been used for calculations of chlorine  $C_Q$  values in solid hydrochlorides on several occasions,<sup>27, 39-41</sup> and also for calculations of  $C_Q$  values of other nuclei.<sup>42</sup>

However, the optimal choice of the cluster for  $C_Q$  calculations may not be obvious. For example, it is very difficult to build a suitable cluster model for alkaline earth chloride hydrates, which form extended three dimensional networks in the solid state.<sup>24</sup> Consequently, it is more efficient to exploit the translational symmetry which is naturally present in many crystals. EFG tensors have been calculated under periodic boundary conditions, for example, using the linearized augmented plane wave (LAPW) method.<sup>43</sup> In the last decade, the projector-augmented

wave (PAW) procedure, which uses plane waves to describe the valence electrons and pseudopotentials to describe the core electrons, has been developed for the prediction of the magnetic resonance parameters under periodic boundary conditions.<sup>44</sup> The wide applications of PAW-based calculations to “NMR crystallography” are well documented.<sup>45-47</sup>

The PAW methodology has been used several times for the calculation of chlorine NMR parameters.<sup>21, 24-25, 28-29, 48</sup> However, the performance for the prediction of EFG tensor parameters for ionic systems is low relative to covalent systems. For example, in a study of amino acid hydrochlorides, it was noticed that the calculated  $C_Q$  values of chloride ions were systematically overestimated by ca. 20 %.<sup>48</sup> A similar systematic overestimation of  $C_Q$  by plane-wave pseudopotential calculations relative to experiment has been reported elsewhere.<sup>21, 24</sup> Furthermore, although there appeared to be a general overestimation, eleven out of fifteen calculated  $C_Q$  values in a systematic study of amino acid hydrochlorides were found to correlate well with the experimental data, but four outliers (L-proline hydrochloride, L-threonine hydrochloride, L-tryptophan hydrochloride and L-histidine hydrochloride monohydrate) were 3–5 MHz away from the values predicted using the linear correlation.<sup>21</sup> In contrast, very good agreement between calculated and experimental  $C_Q$  values was found for group 13 chlorides ( $\text{AlCl}_3$ ,  $\text{GaCl}_3$ ,  $\text{GaCl}_2$ ,  $\text{InCl}_3$ ) with polar covalent bonds between the chlorine atoms and their counterparts.<sup>49</sup> In an attempt to find the cause of the discrepancy between experimental and calculated  $C_Q$  values of chloride anions, the EFG tensors at the covalently bonded chlorine nuclei in organic compounds (experimentally determined by nuclear quadrupolar resonance, NQR) were also calculated and the values were found to be in satisfying agreement with experiment (i.e. within 4 % in most cases). It was concluded at that time that the differences in the observed

and experimental  $^{35}\text{Cl}$  quadrupolar coupling constants of the amino acid hydrochlorides were due to effects of dynamics that were not taken into account in the calculations.<sup>48</sup>

Here, we systematically studied possible sources for the discrepancies between experimental and calculated chlorine  $C_Q$  values. Concretely, we investigated the influence of basis sets, the DFT functional, geometry optimisation, molecular dynamics and nuclear quantum effects. We also revisit the above-mentioned outliers in the correlation of calculated and experimental  $C_Q$  and explain the reasons for the disagreement between the calculations and experiment in several instances.

## Methods

The systems studied (Figure 1) include hydrochlorides of amino acids, hydrochlorides of pharmaceutically important APIs, organic compounds with covalently bound chlorine atoms and an inorganic salt ( $\text{NaClO}_3$ ).

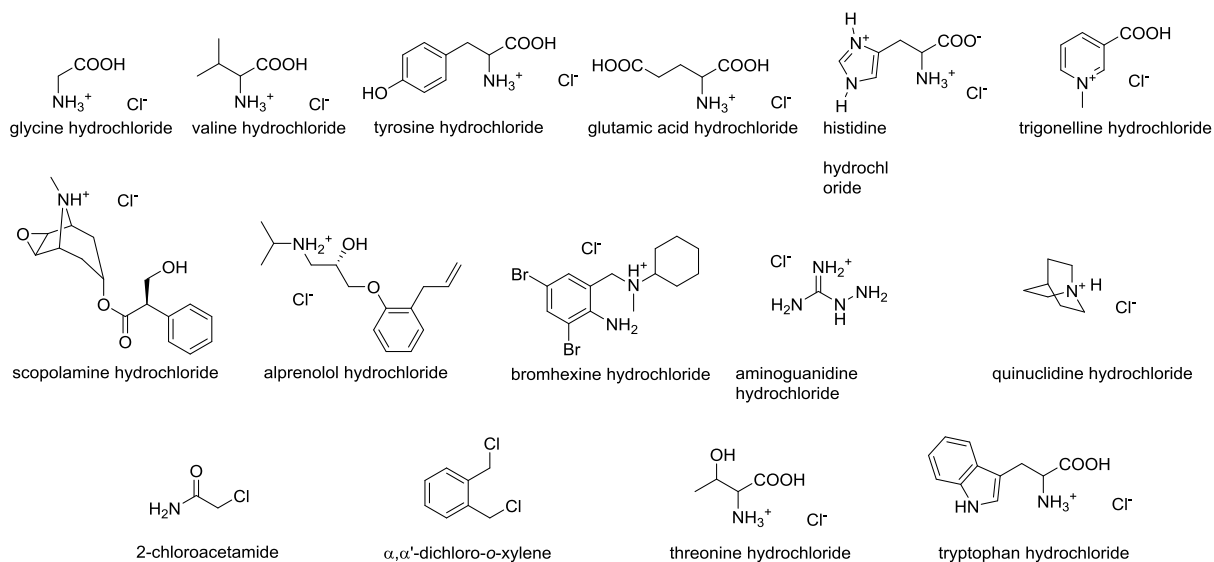


**Figure 1.** The molecular and formula units corresponding to the systems considered herein.

The sample of L-histidine hydrochloride monohydrate used for SS-NMR experiments was obtained from a bottle of this material ( $\geq 99.0\%$ ) which was purchased from Sigma-Aldrich. While not overly sensitive to moisture, and otherwise stable under normal atmospheric conditions, the sample was nevertheless powdered and tightly packed into a 4.0 mm outer diameter  $\text{ZrO}_2$  rotor while under a dry nitrogen atmosphere.

All experimental SS-NMR data were obtained using a Bruker IIIHD NMR spectrometer operating at a  $B_0$  of ca. 11.7 T ( $\nu_0(^1\text{H}) = 499.692$  MHz, and  $\nu_0(^{35}\text{Cl}) = 48.959$  MHz).

Sample purity was verified by collecting  $^1\text{H}$  magic angle spinning (MAS) as well as  $^{13}\text{C}$  and  $^{15}\text{N}$  cross-polarization MAS (CP/MAS) NMR spectra, all of which were in excellent agreement with prior literature findings after accounting for different referencing conventions (see SI, Figures S1 – S3).<sup>50-52</sup> Further details pertaining to the  $^1\text{H}$ ,  $^{13}\text{C}$ , and  $^{15}\text{N}$  SS-NMR experiments can be found in the Supporting Information. The  $^{35}\text{Cl}$  chemical shift reference, and rf field strength, were established using a sample of powdered NaCl under ca. 1.5 kHz MAS, with the shift reference set such that  $\delta_{\text{iso}}(^{35}\text{Cl})$  of solid NaCl was  $-41.11$  ppm.<sup>20</sup> The  $^{35}\text{Cl}$  SS-NMR signal of L-histidine hydrochloride monohydrate was collected at 10 kHz MAS and 283 K using a rotor-synchronized spin echo. During signal acquisition, continuous wave  $^1\text{H}$  decoupling was employed and was such that the  $\nu_{\text{rf}}$  was ca. 70 kHz. As L-histidine hydrochloride monohydrate possesses a non-zero  $^{35}\text{Cl}$  quadrupolar interaction, the resonant rf pulses at the  $^{35}\text{Cl}$  Larmor frequency were scaled by  $1/(I + 1/2) = 1/2$  relative to NaCl, to ensure they were selective for the  $^{35}\text{Cl}$  central transition. The  $^{35}\text{Cl}$  spin-lattice relaxation time (i.e.,  $T_1$ ) was found to be approximately 2 s, thus a 10 s recycle delay was used. After collecting 429 transients, the experiment was stopped, and the time-domain data were subjected a left shift to the echo top,

exponential line broadening of 50 Hz was applied, and finally a fast Fourier transform was used to produce the frequency-domain spectrum. WSolids1 was used to extract the isotropic chemical shift and EFG tensor parameters.<sup>53</sup>

Prior to quantum chemical calculations, atomic coordinates for glycine hydrochloride (refcode GLYHCL), L-valine hydrochloride (VALEHC11), L-glutamic acid hydrochloride (LGLUTA), L-tyrosine hydrochloride (LTYRHC10), L-histidine hydrochloride monohydrate (HISTCM12), trigonelline hydrochloride (QQQAWD01), (-)-scopolamine hydrochloride (KEYSOW), alprenolol hydrochloride (ALPROL), bromhexine hydrochloride (CUXYID), aminoguanidine hydrochloride (AMGUAC02), quinuclidine hydrochloride (QUNCLI), tetrachloro-*p*-benzoquinone (TCBENQ02), tetrachlorohydroquinone (TCLHQU11), 2-chloroacetamide (CLACAM03),  $\alpha,\alpha'$ -dichloro-*o*-xylene (JUZDIR), L-threonine hydrochloride (MOVLOZ) and L-tryptophan hydrochloride (TRYPTC) were taken from the Cambridge Crystallographic Database.<sup>54</sup> Four hydrogen atoms were not placed in the original ALPROL structure, and were thus placed at plausible positions to satisfy the valence of the corresponding carbon atoms. All structures had been obtained in single-crystal studies; the first five crystal structures were determined by neutron diffraction, and the others by X-ray diffraction.

After the appropriate quantum chemical calculation, the principal components  $q_{XX}$ ,  $q_{YY}$ , and  $q_{ZZ}$  of the EFG tensor, defined as  $|q_{ZZ}| \geq |q_{YY}| \geq |q_{XX}|$ , were obtained by diagonalization. The quadrupolar interaction can then be characterized by the nuclear quadrupole coupling constant,  $C_Q = eQq_{ZZ}/h$ , where  $Q$  is the nuclear electric quadrupole moment with the value of  $-0.0817 \cdot 10^{-28} \text{ m}^2$  used for  $^{35}\text{Cl}$ .<sup>55</sup> The quadrupolar asymmetry parameter is defined as  $\eta_Q = (q_{XX} - q_{YY})/q_{ZZ}$ .

We considered three computational approaches: the first was CASTEP calculations (fully periodic, PBE functional, plane waves),<sup>56</sup> the second was CRYSTAL calculations (fully periodic,

various functionals, localized orbitals),<sup>57</sup> and the third was Gaussian09 calculations (clusters, various functionals, localized orbitals).<sup>58</sup>

#### CASTEP calculations

The EFG tensors at the chlorine sites of the infinite crystals were first calculated by the CASTEP program, version 8.0,<sup>56</sup> which uses DFT, pseudopotentials to model the effects of core electrons, and plane waves to describe the valence electrons. Electronic exchange and correlation effects were modelled using the PBE functional,<sup>59</sup> which is a generalized gradient approximation (GGA) exchange-correlation functional. Note that hybrid functionals are prohibitively demanding for plane-wave calculations, and EFG calculations with meta-GGA and hybrid functionals are not implemented in CASTEP. The EFG calculations were performed using the projector-augmented wave approach (PAW)<sup>44, 60</sup> at a plane wave basis set energy cutoff of 600 eV, default ‘on the fly generation’ pseudopotentials, and with a  $k$ -point spacing of  $0.05 \text{ \AA}^{-1}$  over the Brillouin zone via a Monkhorst-Pack grid.<sup>61</sup> Details of the pseudopotential generation in CASTEP are summarized in SI. All atomic positions were optimized at the same computational level prior to the NMR calculations, leading to CASTEP-optimized structures.

DFT-MD simulations of crystalline glycine hydrochloride and  $\text{NaClO}_3$  were run in CASTEP using an  $NVT$  ensemble maintained at a constant temperature of 300 K using a Langevin thermostat, a 0.5 fs integration time step, ultrasoft pseudopotentials,<sup>62</sup> a plane wave basis set energy cutoff energy of 300 eV, and with a minimum  $k$ -point spacing of  $0.1 \text{ \AA}^{-1}$ . The atomic positions were optimized at the same computational level prior to the MD runs. The lattice volumes were fixed to the experimental values, so that the intermolecular interactions were effectively taken into account, and no dispersion correction had to be applied during the MD simulations. It was shown previously that a dispersion correction did not affect the calculated

magnetic shielding values of solid glycine significantly when the lattice parameters were fixed during geometry optimization.<sup>63</sup> The centre of mass in the simulation cell was fixed to ensure that the random initial velocities did not result in translational motions. No symmetry constraints were applied during the MD runs. MD simulations of lengths of 40 ps and 90 ps were performed for glycine hydrochloride and NaClO<sub>3</sub>, respectively. Finally, 391 geometries for the EFG calculations of glycine hydrochloride were selected at  $t = 1.0, 1.1, 1.2 \dots 40.0$  ps and 400 NaClO<sub>3</sub> geometries were selected at  $t = 10.2, 10.4, 10.6 \dots 90.0$  ps. The unit cells of both crystals contained four crystallographically equivalent chlorine atoms ( $Z = 4$ ); therefore, 1564 and 1600 values were averaged for every chemically equivalent site. Averaged principal components of EFG tensors were obtained by averaging each tensor element for a tensor expressed in a fixed Cartesian frame and then diagonalizing the average tensor matrix. The convergence of the calculated  $C_Q$  values is relatively quick (see SI, Figure S4) as the average value oscillates by less than 0.1 MHz (< 1 %) after averaging ca. 200 values. A path integral MD (PIMD) simulation of glycine hydrochloride was performed with the same computational parameters as the conventional DFT-MD described above. A Trotter decomposition of all nuclei into 16 beads (which was found to be satisfactory in previous studies of molecular solids at 300 K<sup>64-65</sup>) and total simulation time of 10 ps were used.

#### CRYSTAL calculations

An alternative approach for the calculation of EFG tensors of fully periodic crystals was performed using the CRYSTAL program,<sup>57</sup> which is also a DFT-based code, but it allows all-electron calculations with localized atomic orbitals used for basis sets. CRYSTAL calculations were performed with Gaussian-type basis sets. First, a convergence test of chlorine EFG tensor eigenvalues with respect to the basis set was performed. For the investigation of the influence of

the functional, CASTEP-optimized structures and 6-31G\*\* basis set was used, since triple valence zeta basis set and other larger basis sets commonly used are not recommended due to their diffusive character.<sup>66</sup> The following functionals were used for the EFG calculations: PBE,<sup>59</sup> hybrid functional B3LYP,<sup>67-68</sup> meta-GGA functional M06L<sup>69</sup> and meta-hybrid functional M06.<sup>70</sup> The effect of geometry optimization of the crystal structure at the same computational level prior to the EFG calculation was tested for selected systems.

### Gaussian09 calculations

The cluster approach for EFG calculations was tested for the glycine hydrochloride and quinuclidine hydrochloride systems. An otherwise isolated cluster of four glycine hydrochloride molecules around the central chloride anion was cut out of the infinite crystal structure (structure in SI) obtained by neutron diffraction without any geometry optimization and 6, 11, 27 or 63 quinuclidine hydrochloride formula units were cut out of the CASTEP-optimized structure (Figure S5 in SI). The same functionals (PBE, B3LYP, M06L and M06) as those used in CRYSTAL calculations and various basis sets were tested. The Gaussian09 program package was used.<sup>58</sup>

## Results

### Basis set dependence

The size of the valence electron basis set in plane-wave calculations is controlled by a single parameter – the energy cutoff, which truncates the basis set to include only plane waves that have smaller kinetic energy values than this parameter. As can be seen in Figure S6 in SI for glycine hydrochloride, the convergence of the absolute value of the quadrupolar coupling constant and the asymmetry parameter in CASTEP calculations is relatively smooth and fast. A

similar convergence profile was observed for quinuclidine hydrochloride (SI, Figure S7). Therefore, we assume an energy cutoff of 600 eV to be reasonable, and this value was used in all other CASTEP PAW-DFT calculations.

However, the convergence of the EFG tensor parameters with respect to the basis set was not straightforward in calculations with the Gaussian-type orbitals used in CRYSTAL and GAUSSIAN09 (Figures 2 and 3). The calculated  $C_Q$  values fluctuate by more than 1 MHz and no convergence trends are apparent. It can be noted, however, that the effect of the functional is even more significant than the basis set. The GGA functional PBE always predicts the highest value of quadrupolar coupling followed by hybrid B3LYP, and meta-GGA and meta-hybrid functionals. It is noticeable that the ‘shape’ of the EFG tensor, as measured by the asymmetry parameter  $\eta_Q$ , is in CRYSTAL almost independent on the functional choice and is close to the CASTEP-calculated value (Figure 2).

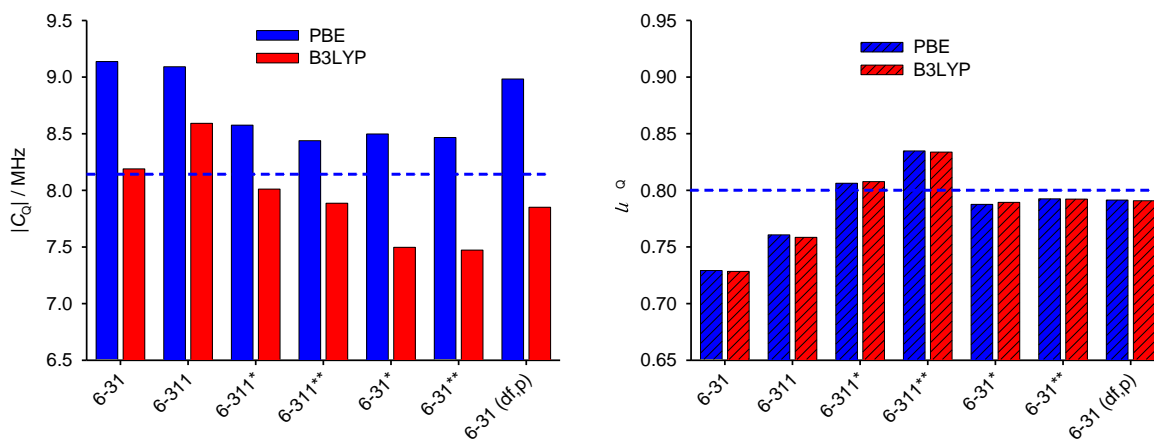


**Figure 2.** Basis set dependence of  $^{35}\text{Cl}$   $|C_Q|$  and  $\eta_Q$  for glycine hydrochloride, calculated with CRYSTAL software using neutron structure without optimization. For comparison, converged CASTEP values established in Figure 2 are indicated by the dashed lines.

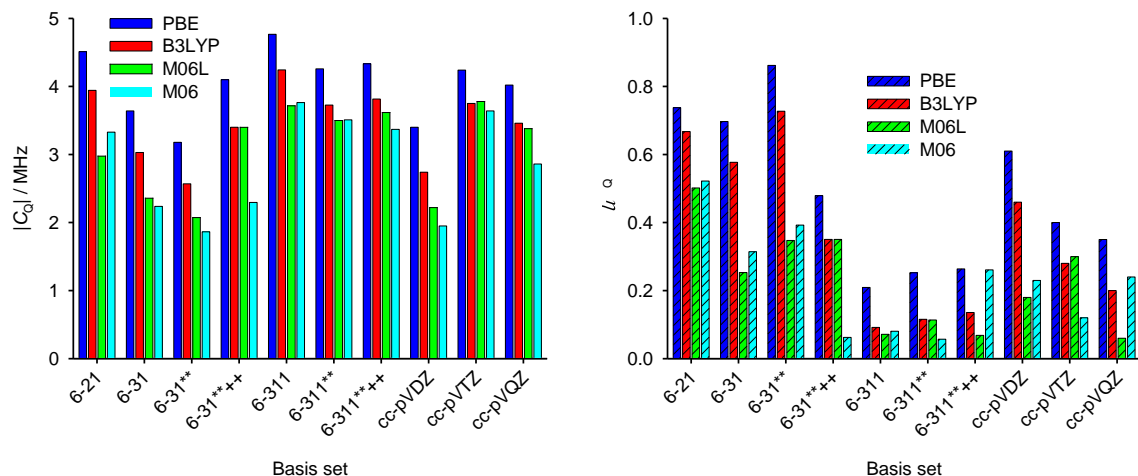


**Figure 3.** Basis set dependence of  $^{35}\text{Cl}$   $|C_Q|$  and  $\eta_Q$  for quinuclidine hydrochloride, Gaussian09 cluster calculations with six quinuclidine formula units in the cluster.

### Geometry optimizations

As noted earlier, the structures used in the present study were originally obtained from either neutron or X-ray diffraction experiments. X-ray diffraction is known for determining the positions of hydrogen atoms with low accuracy and therefore the computational optimization of the hydrogen atom positions in these structures is generally recommended. Optimization of hydrogen atomic positions, when starting from neutron structures, is less critical, which is supported by the generally low differences ( $<0.5$  MHz,  $<15\%$ ) between  $C_Q$  values calculated for the neutron structures without optimization, with optimization of hydrogen atom positions only and with optimization of all atomic positions (Table 1). The asymmetry parameter  $\eta_Q$  is also affected by geometry optimization of neutron structures very slightly only (few percent). However, it has been pointed out recently that molecular dynamics leads to inaccuracies in bond distances even between heavy atoms in neutron diffraction structures (which are generally

acquired at ambient temperature), and optimization of positions of all atoms led to a better agreement between experimental and calculated NMR parameters.<sup>71</sup> We note that a slightly higher difference between chlorine  $C_Q$  and  $\eta_Q$  values calculated for non-optimized and optimized structures is observed for glutamic acid hydrochloride ( $\Delta C_Q = 1.3$  MHz, 30%,  $\Delta\eta_Q = 0.36$ ), but this is not surprising, as it has recently been noted that one of the hydrogen atoms in this crystal structure is probably mis-positioned.<sup>71</sup>

The differences between the calculated  $C_Q$  values for non-optimized and all-atom-optimized structures are much higher in the case of X-ray structures (up to 3.5 MHz), but optimization of the hydrogen atom positions only leads to a good agreement with all-atom-optimized structures in most cases, with the notable exception of alprenolol hydrochloride; this structure was determined with relatively large  $R$  factor of 10.1 % and geometry optimization leads to changes of heavy-atom positions of up to 0.2 Å. A method for semi-empirical refinement of crystal structures has recently been introduced, in which a damping function was optimized to yield geometries that provide good agreement between calculated and experimental  $^{17}\text{O}$  quadrupolar parameters. This optimization method also led to an improvement of calculated chlorine quadrupolar parameters.<sup>72</sup>

The choice of the computational method for the geometry optimization does not appear to play a significant role for the resulting calculated  $C_Q$  values. Differences between chlorine  $C_Q$  values in glycine hydrochloride calculated in CRYSTAL for structures optimized at PBE level in CASTEP and at the same level used for  $C_Q$  calculations in CRYSTAL are always lower than 0.4 MHz (Figure 4). Note also that the geometries optimized in CRYSTAL differed only very slightly from that optimized in CASTEP; the RMSD was always lower than 0.1 Å. On the other hand, the choice of the functional used to calculate  $C_Q$  plays much larger role. Similarly as

discussed above, the GGA functional PBE always predicts the highest  $C_Q$  value, followed by B3LYP, and then the meta-GGA and meta-hybrid functionals. The quadrupolar asymmetry parameters  $\eta_Q$  calculated for glycine hydrochloride after geometry optimization at various computational levels are tabulated in SI (Table S1). It can be seen that the influence of the functional choice on the asymmetry parameter is small and that the asymmetry parameters calculated for CASTEP-optimized structure are almost identical to those calculated for neutron diffraction structure.

**Table 1.** The effect of geometry optimization on calculated  $C_Q(^{35}\text{Cl})$  values.<sup>a</sup>

	CASTEP	CASTEP	CASTEP	Exp <sup>f</sup>	Ref.
	No opt	Opt H	Opt all		
Glycine HCl <sup>b</sup>	-8.18	-8.91	-8.81	6.42(5)	41
Valine HCl <sup>b</sup>	-8.01	-8.16	-8.05	5.89(5)	41
Tyrosine HCl <sup>b</sup>	-3.65	-4.00	-4.18	2.23(2)	73
Glutamic acid HCl <sup>b</sup>	4.35	5.16	5.66	3.61(1)	41
Histidine HCl H <sub>2</sub> O <sup>b</sup>	2.53	2.77	2.63	1.81(2)	this work
Trigonelline HCl <sup>c</sup>	-9.12	-9.62	-9.66	7.50(12)	25
Scopolamine HCl <sup>c</sup>	2.37	5.82	5.85	3.82(3)	25
Alprenolol HCl <sup>c</sup>	<sup>d</sup>	-5.52 <sup>e</sup>	6.74 <sup>e</sup>	5.25(2)	25
Bromhexine HCl <sup>c</sup>	-8.43	-6.40	-7.06	5.80(3)	25
Aminoguanidine HCl <sup>c</sup>	2.29	3.10	3.32	2.0(2)	25
Quinuclidine HCl <sup>c</sup>	-10.1	-6.63	-6.82	5.25(2)	73

<sup>a</sup>CASTEP calculations, PBE functional, 600 eV energy cutoff; <sup>b</sup>Neutron diffraction; <sup>c</sup>X-ray diffraction; <sup>d</sup>Four hydrogen atoms were missing in the ALPROL structure and were added into plausible positions; <sup>e</sup>The asymmetry parameter  $\eta_Q$  of alprenolol HCl is close to 1 leading to sign changes; <sup>f</sup>The sign of  $C_Q$  is not generally available from experiments.

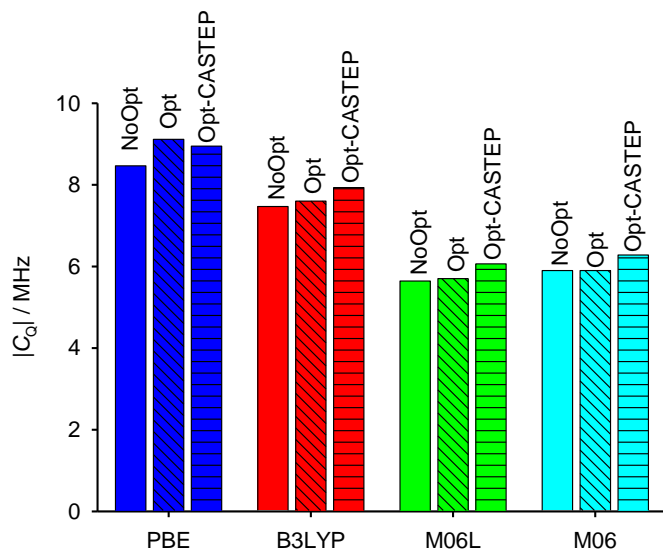


**Figure 4.** The dependence of  $^{35}\text{Cl}$   $|C_Q|$  on the geometry optimization protocol for glycine hydrochloride, calculated with CRYSTAL software. NoOpt: neutron structure without optimization, Opt: optimization of positions of all atoms in CRYSTAL at the same computational level as the EFG tensor calculation, Opt-CASTEP: optimization of positions of all atoms in CASTEP at PBE level prior to CRYSTAL EFG calculations.

The dependence of the calculated quadrupolar coupling and asymmetry parameter on the size of the molecular cluster in Gaussian09 calculations was tested for quinuclidine hydrochloride (Table S2 in SI). It is clear that relatively large clusters of at least 27 formula units have to be used for the ionic system.

### Functional

The choice of the functional used for the EFG tensor calculations appears to most strongly influence the computed values. The  $C_Q$  values of all studied systems calculated using CASTEP

with the PBE exchange-correlation functional, and in CRYSTAL using PBE, B3LYP, M06L and M06 exchange-correlation functionals, are shown in Table 2. In all systems with chlorine present in the form of an anion, the chlorine  $C_Q$  values obtained with PBE functional are higher than those obtained with the B3LYP functional. The M06L and M06 functionals always yield the lowest  $C_Q$  values.

**Table 2.** Experimental and calculated  $^{35}\text{Cl}$  quadrupolar coupling values, in MHz. Positions of all atoms were optimized using CASTEP with the PBE functional. An energy cutoff of 600 eV was used in CASTEP, and the 6-31G\*\* basis set was used in the CRYSTAL calculations.

	CASTEP	CRYSTAL	CRYSTAL	CRYSTAL	CRYSTAL	Exp. <sup>a</sup>	Ref.
	PBE	PBE	B3LYP	M06L	M06		
Glycine HCl	-8.81	-8.95	-7.93	-6.06	-6.28	6.42(5)	41
Valine HCl	-8.05	-8.48	-7.49	-5.86	-6.17	5.89(5)	41
Tyrosine HCl	-4.18	-3.73	-3.13	-2.54	-2.43	2.23(2)	73
Glutamic acid HCl	5.66	4.70	4.10	3.23	3.05	3.61(1)	41
Histidine HCl H <sub>2</sub> O	2.63	3.74	3.13	2.13	2.30	1.81(2)	this work
Trigonelline HCl	-9.66	-9.10	-8.39	-6.84	-7.09	7.50(12)	25
Scopolamine HCl	5.85	6.10	5.26	3.83	4.25	3.82(3)	25
Alprenolol HCl	6.74	-7.00	-5.99	-4.56	-4.87	5.25(2)	25
Bromhexine HCl	-7.06	-7.07	-6.27	-5.37	-5.31	5.80(3)	25
Aminoguanidine HCl	3.32	4.37	3.80	2.81	2.89	2.0(2)	25
Quinuclidine HCl	-6.82	-6.15	-5.47	-4.69	-4.60	5.25(2)	73
NaClO <sub>3</sub>	56.6	59.89	63.60	60.33	62.69	61.7 <sup>b</sup>	74

2-chloroacetamide	-69.06	-67.42	-67.72	-63.75	-64.90	68.30(5)	<sup>23</sup>
$\alpha,\alpha'$ -dichloro- <i>o</i> -xylene	-68.39	-66.56	-66.31	-62.65	-63.41	66.43(8)	<sup>23</sup>
Threonine HCl	-7.11	-7.27	-6.50	-5.35	-5.80	5.4(1)	<sup>21</sup>
Tryptophan HCl	-6.49	-7.12	-6.35	-4.83	-5.30	5.05(4)	<sup>21</sup>

<sup>a</sup>The sign of  $C_Q$  is not generally available from experiments. <sup>b</sup>determined from variable temperature nuclear quadrupolar resonance (NQR) measurements extrapolated to 0 K from variable temperature experiments covering the range 80–450 K.  $C_Q$  at room temperature is ca. 59.9 MHz.<sup>74</sup>

The correlation between CASTEP-PBE calculated and experimental chloride anion  $C_Q$  values fits reasonably well to a straight line with a slope of 1.34 ( $R^2 = 0.92$ , Figure 5, Table 3), which is close to the slope found previously in calculation-experiment correlations for amino acid hydrochlorides.<sup>21</sup> A similar slope is found for CRYSTAL calculations with the PBE functional, but the linear fit is slightly worse ( $R^2 = 0.79$ ); this may be caused by the problematic convergence of the CRYSTAL calculations with respect to the basis set discussed above. CRYSTAL calculations with B3LYP provide a slope of 1.19 and a slightly better correlation coefficient ( $R^2 = 0.85$ ). The meta-GGA and meta-hybrid functionals M06L and M06 provide slopes close to the ideal value of 1 and further improve the correlation coefficient to 0.93 and 0.91, respectively.

As outlined earlier, CASTEP calculations exhibit a systematic convergence with respect to increasing basis set energy cutoff values, but unfortunately are unable to perform EFG tensor calculations with hybrid or meta-GGA functionals. Calculations which use the CRYSTAL software, on the other hand, can be carried out using a variety of modern DFT functionals, but understanding the fashion in which they converge is challenging. It can be, however, noticed (see Table S3 in SI) that the ratio of  $C_Q$  values calculated with two different functionals with the same

basis set is only slightly dependent on the basis set. Therefore, we used CRYSTAL calculations for the determination of a functional scaling factor,  $x$  (e.g.  $x_{\text{B3LYP/PBE}} = C_{\text{Q}}(\text{B3LYP})/C_{\text{Q}}(\text{PBE})$ ), which was then used for scaling the CASTEP-PBE values. We used the 6-31G\*\* basis set in CRYSTAL for the determination of these scaling factors. The scaled  $C_{\text{Q}}$  values fit much better to the linear correlation with experimental data ( $R^2 = 0.94\text{--}0.97$ ). The scaling factors were determined for each compound separately, but they were similar for all systems with chloride anions; the average values and standard deviations are  $x_{\text{B3LYP/PBE}} = 0.88\pm 0.02$ ,  $x_{\text{M06L/PBE}} = 0.69\pm 0.06$  and  $x_{\text{M06/PBE}} = 0.71\pm 0.05$ . The scaling factors determined from cluster calculations of glycine and quinuclidine hydrochlorides in Gaussian09 are similar to those determined in CRYSTAL and are also almost independent on the choice of the basis set (see SI, Tables S4 and S5).

The effect of the functional choice is similar for all three principal components of the EFG tensor and, therefore, the asymmetry parameter  $\eta_{\text{Q}}$ , is only modestly dependent on the computational method in most cases (see SI, Table S6). In an effort to understand the reasons for the large differences between  $C_{\text{Q}}$  values calculated with different functionals, we calculated the EFG tensor of glycine hydrochloride and 2-chloroacetamide with a functional derived from B3LYP functional but with varying admixture of exact exchange from Hartree-Fock theory. The calculations revealed that increasing the portion of the exact exchange significantly (and linearly) reduces the resulting  $C_{\text{Q}}$  value in the case of the ionic system (see SI, Figure S8).

**Table 3.** Comparison between calculated and experimental chloride anion  $C_Q$  values, under the assumption of a linear correlation.  $C_Q(\text{calc}) = a C_Q(\text{exp.})$ : the slope  $a$ , correlation coefficient  $R^2$ , mean absolute deviation  $\langle ||C_Q(\text{calc}) - C_Q(\text{exp.})|| \rangle$ , maximal absolute deviation  $||C_Q(\text{calc}) - C_Q(\text{exp.})||$ .

Method	Functional	Slope $a$	$R^2$	MAE / MHz	MAX / MHz
CASTEP <sup>a</sup>	PBE	1.34	0.92	1.71	2.39
CRYSTAL <sup>b</sup>	PBE	1.35	0.79	1.82	2.59
	B3LYP	1.19	0.85	1.05	1.80
	M06L	0.95	0.93	0.36	0.81
	M06	0.99	0.91	0.42	0.98
CASTEP-scaled <sup>c</sup>	B3LYP/PBE	1.19	0.94	0.96	1.41
	M06L/PBE	0.95	0.95	0.37	0.86
	M06/PBE	0.98	0.97	0.25	0.56

<sup>a</sup>An energy cutoff of 600 eV was used in CASTEP calculations; <sup>b</sup>6-31G\*\* basis set was used in CRYSTAL calculations; <sup>c</sup>CASTEP-PBE calculation scaled by a factor obtained from CRYSTAL calculations with PBE and a different functional.

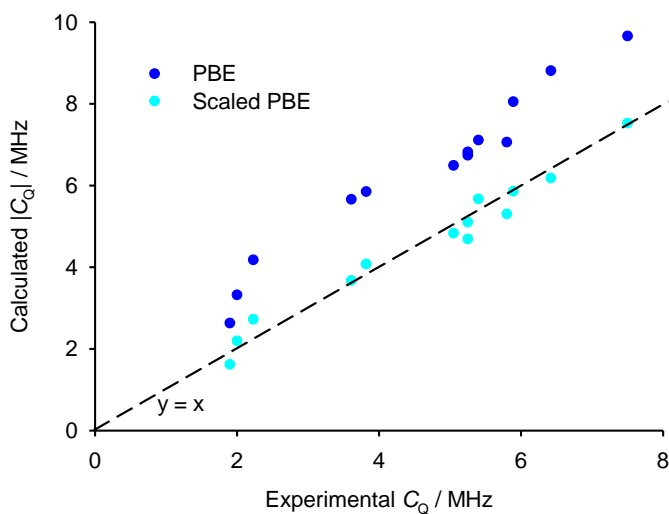


**Figure 5.** The correlation between experimental and calculated chloride anion  $|C_Q(^{35}\text{Cl})|$  values. CASTEP-optimized structures, CASTEP calculations with PBE functional (dark blue); CASTEP calculations with PBE functional, subsequently scaled by M06/PBE factor obtained by CRYSTAL calculations (cyan).

The agreement between experimental and calculated  $C_Q$  values for covalently bound chlorine atoms is reasonably good even with the PBE functional, and the effects of the choice of functional on the calculated  $C_Q$  value is about a few per cent. For example, the chlorine  $C_Q$  in 2-chloroacetamide calculated in CASTEP is 69.1 MHz and CRYSTAL calculations with PBE and M06 functionals provide  $C_Q$  values of 67.4 and 64.9 MHz, respectively. All these values are relatively close to the experimental value of 68.3 MHz and the scaling factor  $x_{\text{M06/PBE}}$  determined in CRYSTAL is 0.96, i.e. much closer to 1 than the scaling factor determined for ionic systems. Note, however, that although the relative agreement of calculated and experimental  $C_Q$  values for systems with covalently bound chlorine is good, the absolute deviations are in the order of a few MHz, which would be considered very large in ionic systems with typical  $C_Q$  values lower than

10 MHz. Similarly good agreement between experimental and calculated values obtained with all studied functionals is observed for  $\alpha,\alpha'$ -dichloro-*o*-xylene (Table 2) and for three other systems which possess covalently bound chlorine atoms (SI, Table S7). Very good agreement between CASTEP-calculated  $C_Q$  values and experiment has also been observed previously in a study of group 13 chlorides with polar covalent bonds between chlorine and the metal atoms; the calculated values were always identical to the experimental ones within the experimental error.<sup>49</sup>

### **Fast molecular dynamics and nuclear quantum effects**

In a previous work, the influence of fast molecular dynamics (fs – ps time scales) on the magnitudes of NMR observable parameters was studied by a combination of DFT-MD simulations with NMR calculations.<sup>71</sup> The influence of molecular dynamics on magnetic shielding and EFG tensors was divided into two aspects. First, the molecular motion has a direct impact on the instantaneous magnitudes of the NMR tensors and second, the orientation of the tensors can also change, which leads to a more spherically averaged tensor and consequently to lower calculated  $C_Q$  values. The sign of the first contribution is dependent on the local environment, while the re-orientation component always decreases the magnitude of the chemical shielding anisotropy and the quadrupolar coupling constant.

Here, we performed DFT-MD simulations of  $\text{NaClO}_3$  and glycine hydrochloride, and calculated EFG tensors for 400 and 391 snapshot geometries, respectively. The contribution of fast dynamics to the instantaneous quadrupolar coupling values is estimated by averaging the magnitudes of  $C_Q$  calculated for every snapshot, while the overall effect of dynamics is obtained by averaging the individual EFG tensor components and calculating the eigenvalues of the average tensor (Table S8 in the SI). For  $\text{NaClO}_3$ , both above-mentioned dynamic contributions

slightly decrease  $C_Q$ , while dynamics in glycine hydrochloride increases the instantaneous magnitude of  $C_Q$ , but this effect is compensated by the EFG tensor re-orientation, leading to a very small overall effect of fast dynamics on the  $C_Q$  value. The overall effect of fast dynamics on  $\text{NaClO}_3$  chlorine  $C_Q$ , determined as the difference between the  $C_Q$  value calculated for the geometry optimized structure and the value obtained from the average EFG tensor, is 1.6 MHz, which agrees very well with the value estimated from variable temperature NQR experiments (1.5 MHz).<sup>74</sup> The asymmetry parameter  $\eta_Q$  ( $\eta_Q = 0.00$ ) is not affected by the molecular dynamics.

Nuclear quantum effects (NQEs), which are not captured by conventional MD simulations, may be also important for EFG tensor calculations. It has been shown that NQEs may significantly influence the magnitudes of chemical shifts and quadrupolar coupling values in systems with strong hydrogen bonds.<sup>65, 75</sup> We performed a PIMD simulation for glycine hydrochloride. Fluctuations of hydrogen atoms in the PIMD simulations are larger than in the DFT-MD simulation (root mean square deviations of the atomic positions are 0.42 and 0.37 Å for PIMD and MD, respectively), which is reflected in larger fluctuations of the instantaneous  $C_Q(^{35}\text{Cl})$  values. The calculated average magnitude of  $C_Q$  is 12.04 MHz, but the re-orientation of the EFG tensor leads to a partial compensation of the effect of the changing environment. Both MD and PIMD averaging of the EFG tensors also leads to a decrease of the asymmetry parameter  $\eta_Q$  ( $\eta_Q = 0.80$  for the geometry optimized structure,  $\eta_Q = 0.70$  for MD averaging and  $\eta_Q = 0.65$  for PIMD averaging, experimental value is  $\eta_Q = 0.61$ ). Although larger scale motions in the crystal, such as librational motion of molecular domains, are not captured by the short PIMD simulation, these might lead to a further decrease in the calculated  $C_Q$  value due to EFG tensor averaging. However, it is likely that the effect of longer timescale dynamics ( $\mu\text{s}$ ) in these

‘rigid’ solids, without any sign of static or dynamic disorder, will be limited and will not be the main reason for the discrepancies between experimental and calculated  $C_Q$  values.

### **Re-visiting previous systems**

In a systematic study of amino acid hydrochlorides, eleven out of fifteen calculated  $C_Q$  values correlated well with the experimental data, but four outliers (proline hydrochloride, L-threonine hydrochloride, L-tryptophan hydrochloride and L-histidine hydrochloride monohydrate) were found to be 3–5 MHz away from the linear correlation.<sup>21</sup> We now address each of these systems in turn.

Proline hydrochloride. L-proline was used to prepare the hydrochloride salt used for NMR experiments.<sup>41</sup> However, the crystal structure DLPROL deposited in CCSD was used for the EFG tensor calculation in ref.<sup>21</sup>; this crystal structure corresponds to a racemic mixture of D- and L-proline and it will therefore be different from the crystal structure of the pure enantiomer. Hence, this structure cannot be used for the prediction of  $C_Q$ .

L-Threonine hydrochloride. A newly determined X-ray structure of threonine hydrochloride (deposited in CCSD under refcode: MOVLOZ) was used for the calculation of the  $^{35}\text{Cl}$   $C_Q$  value. When inspecting the structure, the distance between the hydroxyl oxygen on  $\text{C}\beta$  and the chloride anion is 3.13 Å, which is suitable for hydrogen bonding. However, the hydroxyl O–H bond is oriented in a different direction and the hydrogen is not involved in any hydrogen bonding interaction. The chlorine quadrupolar coupling constant calculated for this structure after geometry optimization (10.6 MHz) is, indeed, far from the experimental value (5.4 MHz). However, a different structure of threonine hydrochloride is also in the CCSD (refcode: MOVLOZ01),<sup>76</sup> which is almost identical to the MOVLOZ structure but the hydroxyl hydrogen

is now involved in the hydrogen bond with the chlorine atom. The calculated chlorine  $C_Q$  for the MOVLOZ01 structure is 3.5 MHz lower and is close to the linear correlation between experimental and PBE calculated magnitudes of  $C_Q$ . Note that a geometry optimization of the original MOVLOZ structure does not lead to a change in the orientation of the OH group, but when the orientation is manually changed to be suitable for the hydrogen bonding and the structure is geometry optimized (Figure S9 in SI), the resulting energy normalized per threonine molecule is 0.4 eV (39 kJ/mol) lower than in the original geometry-optimized structure. Based on prior computational studies, an energy difference this large is strong evidence that the original structure is unlikely to be correct.<sup>77-78</sup> This is consistent with other cases where “NMR crystallography” studies have identified mis-positioned hydrogen atoms in OH groups.<sup>79-81</sup>

L-Histidine hydrochloride monohydrate. This system is the only example where the  $C_Q$  value calculated using the PBE functional under CASTEP was lower (2.72 MHz) than the experimental one (4.59 MHz).<sup>21</sup> The sample for NMR experiments potentially contained impurities, which may have affected the spectral fitting,<sup>40</sup> but the presence of the impurities probably cannot explain large deviations from the calculated  $C_Q$  value. Recent measurements of the  $C_Q(^{35}\text{Cl})$  value in histidine hydrochloride monohydrate using one-dimensional  $^{35}\text{Cl}$  NMR and two-dimensional proton-detected  $^{35}\text{Cl}$ - $^1\text{H}$  correlation NMR experiments gave chlorine a  $C_Q$  of 1.8–2 MHz,<sup>26</sup> which fits well the correlation between experimental and calculated  $C_Q$ . While the range of values is useful as a guide, it is expected that direct detection measurements *via* the spin-echo  $^{35}\text{Cl}$  MAS NMR experiment would be well-suited for the precise measurement of this parameter. Indeed, using the spin-echo pulse sequence under 10 kHz MAS, we precisely measured the  $^{35}\text{Cl}$  EFG tensor, in addition to the isotropic chlorine chemical shift of this system (Figure 6).

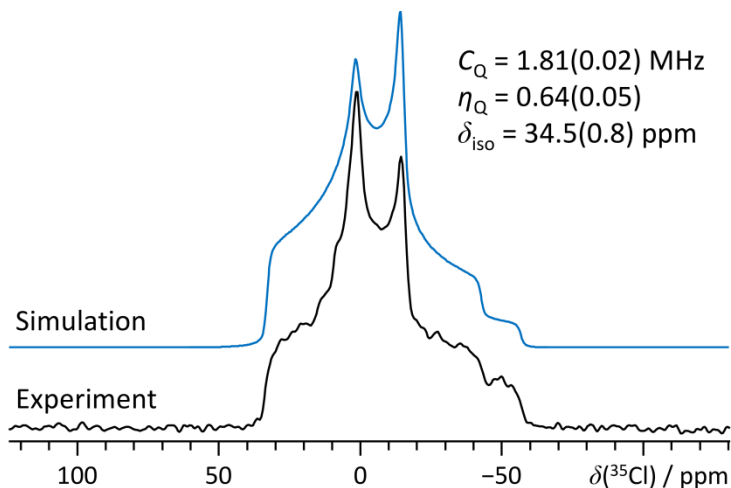


**Figure 6.** Experimental  $^{35}\text{Cl}$  MAS NMR spectrum of L-histidine hydrochloride monohydrate, acquired using a rotor-synchronized spin-echo pulse sequence,  $\nu_{\text{MAS}} = 10$  kHz, and  $B_0 = 11.7$  T. Extracted parameter values (with errors in parentheses) can be found inset on the right. Additional details can be found in the experimental section.

L-Tryptophan hydrochloride. Our calculation of the  $C_Q(^{35}\text{Cl})$  value in tryptophan hydrochloride differs from that published previously<sup>21</sup> for unknown reasons. The published value (11.62 MHz, obtained after optimization of hydrogen atoms positions, 450 eV energy cutoff) was substantially higher than the experimental one (5.05 MHz). Our calculations using a 600 eV energy cutoff and optimized positions of all atoms (-6.49 MHz) or hydrogen atoms only (-6.40 MHz) agree well with the correlation between experimental and PBE calculated quadrupolar couplings and the  $^{35}\text{Cl}$   $C_Q$  value calculated with a 450 eV energy cutoff is almost identical to that with 600 eV cutoff (-6.38 MHz, positions of H atoms optimized only).

## Conclusions

In a systematic fashion, we have attempted to understand and explain the disagreement between experimental and DFT-calculated chlorine quadrupolar coupling constants for ionic chlorides in crystalline systems. Specifically, we probed the influence of the basis set, the functional, the geometry optimization protocol, fast time scale molecular dynamics and nuclear quantum effects.

The choice of the exchange-correlation functional was unequivocally identified as the most critical computational parameter for the calculation of the quadrupolar coupling constants associated with chloride anions. The GGA functional PBE systematically overestimates the  $C_Q$  values, while the values of this parameter calculated using meta-GGA M06L and meta-hybrid M06 functionals is significantly lower. The hybrid B3LYP functional performance is consistently found to be in-between the PBE and M06-type functionals. Interestingly, in relative terms, the effect of the choice of the functional is much lower for covalently bound chlorine atoms in organic compounds. The choice of the functional is much less critical for the calculated ‘shape’ of the EFG tensor, as expressed by the asymmetry parameter  $\eta_Q$ .

The choice of the basis set and the geometry optimization procedure followed is also found to be important, but has a more modest effect on the calculated values than the functional choice. The convergence of plane-wave calculations with respect to basis set size is relatively smooth and easily controlled by the  $E_{\text{cutoff}}$  parameter, as expected. The convergence of Gaussian-type basis sets is, on the other hand, not straightforward, but one advantage of these basis sets is that they can be more efficiently used in EFG calculations using modern functionals beyond the GGA level in currently available software.

We propose a method of scaling the well-converged EFG tensors which have resulted from plane-wave calculations with a factor obtained as the PBE/M06 ratio of the  $C_Q$  value determined for the given system with a Gaussian-type basis set. For the benchmark systems considered at present, this approach leads to a good agreement between calculated and experimental quadrupolar coupling values and may thus be employed in a straightforward manner in future NMR crystallography studies of chloride containing systems.

The effect of fast molecular dynamics on the chlorine quadrupolar coupling values was investigated by a combination of DFT-MD simulations and calculations of the EFG tensors for geometries taken from simulation snapshots. For  $\text{NaClO}_3$ , fast dynamics leads to a ca. 4 % decrease in the average  $C_Q$  value, which is in agreement with the previously observed temperature dependence of the NQR frequency of  $\text{NaClO}_3$ . For glycine hydrochloride, a PIMD simulation, which takes account of nuclear quantum effects, was performed. The fluctuations of atomic positions and of the calculated  $C_Q$  values are larger relative to MD-DFT in this simulation (the average  $C_Q$  value was 1 MHz higher than that calculated for the geometry optimized structure), but the overall effects of fast dynamics / nuclear delocalisation were consistently much smaller than the choice of the functional used for the calculation.

We find that the influence of the functional choice on the calculated chlorine quadrupolar coupling constants can be suppressed, by using the scaling factors described above. This results in  $C_Q$  values which agree well with experiment, and our finding paves the way for chlorine to be used in NMR crystallography studies in a similar way as other commonly used nuclei. The comparison of experimental and calculated  $C_Q$  values can, for example, be used to discriminate between two crystal structures determined by X-ray diffraction, as we demonstrated for L-threonine hydrochloride.

## ASSOCIATED CONTENT

**Supporting Information.** The Supporting Information is available free of charge on the ACS Publications website at DOI:

Experimental  $^1\text{H}$ ,  $^{13}\text{C}$  and  $^{15}\text{N}$  NMR spectra of histidine hydrochloride monohydrate, additional details of computational methods, additional figures.

## AUTHOR INFORMATION

### Corresponding Author

\*Email: dracinsky@uochb.cas.cz

## ACKNOWLEDGMENT

The work has been supported by the Czech Science Foundation (grant no. 15-11223S).

## REFERENCES

1. Gribble, G. W. Naturally Occurring Organohalogen Compounds. *Accounts Chem. Res.* **1998**, *31*, 141-152.
2. Gribble, G. W. A Recent Survey of Naturally Occurring Organohalogen Compounds. *Environ. Chem.* **2015**, *12*, 396-405.
3. Jentsch, T. J.; Stein, V.; Weinreich, F.; Zdebik, A. A. Molecular Structure and Physiological Function of Chloride Channels. *Physiol. Rev.* **2002**, *82*, 503-568.
4. Schmittinger, P.; Florkiewicz, T.; Curlin, L. C.; Lüke, B.; Scannell, R.; Navin, T.; Zelfel, E.; Bartsch, R. Chlorine. *Ullmann's Encyclopedia of Industrial Chemistry*, Wiley-VCH Verlag GmbH & Co. KGaA: 2000.

5. Greenwood, N. N.; Earnshaw, A. *Chemistry of the Elements*. Elsevier Butterworth-Heinemann: Oxford, 1997.
6. Whitfield, R.; Brown, F. *The Benefits of Chlorine Chemistry in Pharmaceuticals in the United States and Canada.*, <https://chlorine.americanchemistry.com/Chlorine-Benefits/> (accessed February 15, 2017).
7. Wermuth, C. G.; Stahl, P. H. Introduction. In *Handbook of Pharmaceutical Salts: Properties, Selection and Use*, Stahl, P. H.; Wermuth, C. G., Eds. Wiley-VCH: Weinheim, 2002; pp 1-7.
8. Bansal, A. K.; Kumar, L.; Amin, A. Salt Selection in Drug Development. *Pharmaceutical Technology* **2008**, *32*, <http://www.pharmtech.com/salt-selection-drug-development> (accessed February 15, 2017).
9. Metrangolo, P.; Meyer, F.; Pilati, T.; Resnati, G.; Terraneo, G. Halogen Bonding in Supramolecular Chemistry. *Angew. Chem. Int. Ed.* **2008**, *47*, 6114-6127.
10. Harris, R. K. NMR Studies of Organic Polymorphs & Solvates. *Analyst* **2006**, *131*, 351-373.
11. Dračinský, M.; Buděšínský, M.; Warzajtis, B.; Rychlewska, U. Solution and Solid-State Effects on NMR Chemical Shifts in Sesquiterpene Lactones: NMR, X-ray, and Theoretical Methods. *J. Phys. Chem. A* **2012**, *116*, 680-688.
12. Apperley, D. C.; Harris, R. K.; Hodgkinson, P. *Solid-State NMR: Basic Principles & Practice*. Momentum Press: New York, 2012.

13. Agarwal, V.; Penzel, S.; Szekely, K.; Cadalbert, R.; Testori, E.; Oss, A.; Past, J.; Samoson, A.; Ernst, M.; Bockmann, A.; Meier, B. H. De Novo 3D Structure Determination from Sub-milligram Protein Samples by Solid-State 100 kHz MAS NMR Spectroscopy. *Angew. Chem. Int. Ed.* **2014**, *53*, 12253-12256.
14. Kobayashi, T.; Mao, K.; Paluch, P.; Nowak-Krol, A.; Sniechowska, J.; Nishiyama, Y.; Gryko, D. T.; Potrzebowski, M. J.; Pruski, M. Study of Intermolecular Interactions in the Corrole Matrix by Solid-State NMR under 100 kHz MAS and Theoretical Calculations. *Angew. Chem. Int. Ed.* **2013**, *52*, 14108-14111.
15. Wooten, E. W.; Mueller, K. T.; Pines, A. New Angles in Nuclear-Magnetic-Resonance Sample Spinning. *Acc. Chem. Res.* **1992**, *25*, 209-215.
16. Samoson, A.; Lippmaa, E.; Pines, A. High-Resolution Solid-State NMR Averaging of 2nd-Order Effects by Means of a Double-Rotor. *Mol. Phys.* **1988**, *65*, 1013-1018.
17. Mueller, K. T.; Sun, B. Q.; Chingas, G. C.; Zwanziger, J. W.; Terao, T.; Pines, A. Dynamic-Angle Spinning of Quadrupolar Nuclei. *J. Magn. Reson.* **1990**, *86*, 470-487.
18. Medek, A.; Harwood, J. S.; Frydman, L. Multiple-Quantum Magic-Angle Spinning NMR: A New Method for the Study of Quadrupolar Nuclei in Solids. *J. Am. Chem. Soc.* **1995**, *117*, 12779-12787.
19. Widdifield, C. M.; Chapman, R. P.; Bryce, D. L. Chlorine, Bromine, and Iodine Solid-State NMR Spectroscopy. *Annu. Rep. NMR Spectrosc.* **2009**, *66*, 195-326.
20. Chapman, R. P.; Widdifield, C. M.; Bryce, D. L. Solid-State NMR of Quadrupolar Halogen Nuclei. *Prog. Nucl. Magn. Reson. Spectrosc.* **2009**, *55*, 215-237.

21. Chapman, R. P.; Hiscock, J. R.; Gale, P. A.; Bryce, D. L. A Solid-State  $^{35/37}\text{Cl}$  NMR Study of a Chloride Ion Receptor and a GIPAW-DFT Study of Chlorine NMR Interaction Tensors in Organic Hydrochlorides. *Can. J. Chem.* **2011**, *89*, 822-834.
22. Szell, P. M. J.; Bryce, D. L. Recent Advances in Chlorine, Bromine, and Iodine Solid-State NMR Spectroscopy. *Annu. Rep. NMR Spectrosc.* **2015**, *84*, 115-162.
23. Perras, F. A.; Bryce, D. L. Direct Investigation of Covalently Bound Chlorine in Organic Compounds by Solid-State  $^{35}\text{Cl}$  NMR Spectroscopy and Exact Spectral Line-Shape Simulations. *Angew. Chem. Int. Ed.* **2012**, *51*, 4227-4230.
24. Bryce, D. L.; Bultz, E. B. Alkaline Earth Chloride Hydrates: Chlorine Quadrupolar and Chemical Shift Tensors by Solid-State NMR Spectroscopy and Plane Wave Pseudopotential Calculations. *Chem. Eur. J.* **2007**, *13*, 4786-4796.
25. Hildebrand, M.; Hamaed, H.; Namespetra, A. M.; Donohue, J. M.; Fu, R. Q.; Hung, I.; Gan, Z. H.; Schurko, R. W.  $^{35}\text{Cl}$  Solid-State NMR of HCl Salts of Active Pharmaceutical Ingredients: Structural Prediction, Spectral Fingerprinting and Polymorph Recognition. *CrystEngComm* **2014**, *16*, 7334-7356.
26. Pandey, M. K.; Kato, H.; Ishii, Y.; Nishiyama, Y. Two-Dimensional Proton-Detected  $^{35}\text{Cl}/^1\text{H}$  Correlation Solid-State NMR Experiment under Fast Magic Angle Sample Spinning: Application to Pharmaceutical Compounds. *Phys. Chem. Chem. Phys.* **2016**, *18*, 6209-6216.
27. Hamaed, H.; Pawlowski, J. M.; Cooper, B. F. T.; Fu, R. Q.; Eichhorn, S. H.; Schurko, R. W. Application of Solid-State  $^{35}\text{Cl}$  NMR to the Structural Characterization of Hydrochloride Pharmaceuticals and their Polymorphs. *J. Am. Chem. Soc.* **2008**, *130*, 11056-11065.

28. Vogt, F. G.; Williams, G. R.; Strohmeier, M.; Johnson, M. N.; Copley, R. C. B. Solid-State NMR Analysis of a Complex Crystalline Phase of Ronacaleret Hydrochloride. *J. Phys. Chem. B* **2014**, *118*, 10266-10284.
29. Namespetra, A. M.; Hirsh, D. A.; Hildebrand, M. P.; Sandre, A. R.; Hamaed, H.; Rawson, J. M.; Schurko, R. W. <sup>35</sup>Cl Solid-State NMR Spectroscopy of HCl Pharmaceuticals and their Polymorphs in Bulk and Dosage Forms. *CrystEngComm* **2016**, *18*, 6213-6232.
30. Hirsh, D. A.; Rossini, A. J.; Emsley, L.; Schurko, R. W. <sup>35</sup>Cl Dynamic Nuclear Polarization Solid-State NMR of Active Pharmaceutical Ingredients. *Phys. Chem. Chem. Phys.* **2016**, *18*, 25893-25904.
31. Widdifield, C. M.; Bryce, D. L. A Multinuclear Solid-State Magnetic Resonance and GIPAW DFT Study of Anhydrous Calcium Chloride and its Hydrates. *Can. J. Chem.* **2011**, *89*, 754-763.
32. Attrell, R. J.; Widdifield, C. M.; Korobkov, I.; Bryce, D. L. Weak Halogen Bonding in Solid Haloanilinium Halides Probed Directly via Chlorine-35, Bromine-81, and Iodine-127 NMR Spectroscopy. *Cryst. Growth Des.* **2012**, *12*, 1641-1653.
33. Viger-Gravel, J.; Leclerc, S.; Korobkov, I.; Bryce, D. L. Direct Investigation of Halogen Bonds by Solid-State Multinuclear Magnetic Resonance Spectroscopy and Molecular Orbital Analysis. *J. Am. Chem. Soc.* **2014**, *136*, 6929-6942.
34. Szell, P. M. J.; Bryce, D. L. <sup>35</sup>Cl Solid-State NMR and Computational Study of Chlorine Halogen Bond Donors in Single-Component Crystalline Chloronitriles. *J. Phys. Chem. C* **2016**, *120*, 11121-11130.

35. Brinkmann, C.; Faske, S.; Vogel, M.; Nilges, T.; Heuer, A.; Eckert, H. Silver Ion Dynamics in the Ag<sub>5</sub>Te<sub>2</sub>Cl-Polymorphs Revealed by Solid State NMR Lineshape and two- and three-Time Correlation Spectroscopies. *Phys. Chem. Chem. Phys.* **2006**, *8*, 369-378.
36. Czupinski, O.; Wojtas, M.; Zaleski, J.; Jakubas, R.; Medycki, W. Structure and Properties of 2-Cyanopyridinium Perchlorate [2-CNPyH][ClO<sub>4</sub>]. *J. Phys.: Condens. Matter* **2006**, *18*, 3307-3324.
37. Trill, H.; Eckert, H.; Srdanov, V. I. Mixed Halide Sodalite Solid Solution Systems. Hydrothermal Synthesis and Structural Characterization by Solid State NMR. *J. Phys. Chem. B* **2003**, *107*, 8779-8788.
38. Sandland, T. O.; Du, L. S.; Stebbins, F.; Webster, J. D. Structure of Cl-Containing Silicate and Aluminosilicate Glasses: A <sup>35</sup>Cl MAS-NMR study. *Geochim. Cosmochim. Acta* **2004**, *68*, 5059-5069.
39. Bryce, D. L.; Sward, G. D. Chlorine-35/37 NMR Spectroscopy of Solid Amino Acid Hydrochlorides: Refinement of Hydrogen-Bonded Proton Positions Using Experiment and Theory. *J. Phys. Chem. B* **2006**, *110*, 26461-26470.
40. Chapman, R. P.; Bryce, D. L. A High-Field Solid-State <sup>35/37</sup>Cl NMR and Quantum Chemical Investigation of the Chlorine Quadrupolar and Chemical Shift Tensors in Amino Acid Hydrochlorides. *Phys. Chem. Chem. Phys.* **2007**, *9*, 6219-6230.
41. Bryce, D. L.; Sward, G. D.; Adiga, S. Solid-State <sup>35/37</sup>Cl NMR Spectroscopy of Hydrochloride Salts of Amino Acids Implicated in Chloride Ion Transport Channel Selectivity: Opportunities at 900 MHz. *J. Am. Chem. Soc.* **2006**, *128*, 2121-2134.

42. Holmes, S. T.; Bai, S.; Iuliucci, R. J.; Mueller, K. T.; Dybowski, C. Calculations of Solid-State  $^{43}\text{Ca}$  NMR Parameters: A Comparison of Periodic and Cluster Approaches and an Evaluation of DFT Functionals. *J. Comput. Chem.* **2017**, *38*, 949-956.
43. Blaha, P.; Schwarz, K.; Dederichs, P. H. First Principles Calculation of the Electric-Field Gradient in Hcp Metals. *Phys. Rev. B* **1988**, *37*, 2792-2796.
44. Pickard, C. J.; Mauri, F. All-Electron Magnetic Response with Pseudopotentials: NMR Chemical Shifts. *Phys. Rev. B* **2001**, *6324*, 245101.
45. Harris, R. K.; Hodgkinson, P.; Pickard, C. J.; Yates, J. R.; Zorin, V. Chemical Shift Computations on a Crystallographic Basis: Some Reflections and Comments. *Magn. Reson. Chem.* **2007**, *45*, S174-S186.
46. Bonhomme, C.; Gervais, C.; Babonneau, F.; Coelho, C.; Pourpoint, F.; Azais, T.; Ashbrook, S. E.; Griffin, J. M.; Yates, J. R.; Mauri, F.; Pickard, C. J. First-Principles Calculation of NMR Parameters Using the Gauge Including Projector Augmented Wave Method: A Chemist's Point of View. *Chem. Rev.* **2012**, *112*, 5733-5779.
47. Ashbrook, S. E.; McKay, D. Combining Solid-State NMR Spectroscopy with First-Principles Calculations - a Guide to NMR Crystallography. *Chem. Commun.* **2016**, *52*, 7186-7204.
48. Gervais, C.; Dupree, R.; Pike, K. J.; Bonhomme, C.; Profeta, M.; Pickard, C. J.; Mauri, F. Combined First-Principles Computational and Experimental Multinuclear Solid-State NMR Investigation of Amino Acids. *J. Phys. Chem. A* **2005**, *109*, 6960-6969.

49. Chapman, R. P.; Bryce, D. L. Application of Multinuclear Magnetic Resonance and Gauge-Including Projector-Augmented-Wave Calculations to the Study of Solid Group 13 Chlorides. *Phys. Chem. Chem. Phys.* **2009**, *11*, 6987-6998.
50. Rossini, A. J.; Schlagnitweit, J.; Lesage, A.; Emsley, L. High-Resolution NMR of Hydrogen in Organic Solids by DNP Enhanced Natural Abundance Deuterium Spectroscopy. *J. Magn. Reson.* **2015**, *259*, 192-198.
51. Siegel, R.; Trebosc, J.; Amoureux, J. P.; Gan, Z. 3D  $^1\text{H}$ - $^{13}\text{C}$ - $^{14}\text{N}$  Correlation Solid-State NMR Spectrum. *J. Magn. Reson.* **2008**, *193*, 321-325.
52. Kalakewich, K.; Iulicci, R.; Mueller, K. T.; Eloranta, H.; Harper, J. K. Monitoring the Refinement of Crystal Structures with  $^{15}\text{N}$  Solid-State NMR Shift Tensor Data. *J. Chem. Phys.* **2015**, *143*, 194702.
53. Eichele, K.; Wasylishen, R. E. *Wsolids1, Version 1.19.11*, Universität Tübingen: Tübingen, 2009.
54. Allen, F. H. The Cambridge Structural Database: A Quarter of a Million Crystal Structures and Rising. *Acta Cryst. B* **2002**, *58*, 380-388.
55. Pyykkö, P. Year-2008 Nuclear Quadrupole Moments. *Mol. Phys.* **2008**, *106*, 1965-1974.
56. Clark, S. J.; Segall, M. D.; Pickard, C. J.; Hasnip, P. J.; Probert, M. J.; Refson, K.; Payne, M. C. First Principles Methods Using CASTEP. *Z. Kristallogr.* **2005**, *220*, 567-570.
57. Dovesi, R.; Orlando, R.; Erba, A.; Zicovich-Wilson, C. M.; Civalleri, B.; Casassa, S.; Maschio, L.; Ferrabone, M.; De La Pierre, M.; D'Arco, P.; Noel, Y.; Causa, M.; Rerat, M.;

Kirtman, B. Crystal14: A Program for the Ab Initio Investigation of Crystalline Solids. *Int. J. Quantum Chem.* **2014**, *114*, 1287-1317.

58. Frisch, M. J.; Trucks, G. W.; Schlegel, H. B.; Scuseria, G. E.; Robb, M. A.; Cheeseman, J. R.; Scalmani, G.; Barone, V.; Mennucci, B.; Petersson, G. A., et al. *Gaussian 09, Revision A.02*, Gaussian, Inc.: Wallingford CT, 2009.

59. Perdew, J. P.; Burke, K.; Ernzerhof, M. Generalized Gradient Approximation Made Simple. *Phys. Rev. Lett.* **1996**, *77*, 3865-3868.

60. Yates, J. R.; Pickard, C. J.; Mauri, F. Calculation of NMR Chemical Shifts for Extended Systems Using Ultrasoft Pseudopotentials. *Phys. Rev. B* **2007**, *76*, 024401.

61. Monkhorst, H. J.; Pack, J. D. Special Points for Brillouin-Zone Integrations. *Phys. Rev. B* **1976**, *13*, 5188-5192.

62. Vanderbilt, D. Soft Self-Consistent Pseudopotentials in a Generalized Eigenvalue Formalism. *Phys. Rev. B* **1990**, *41*, 7892-7895.

63. Dračinský, M.; Bouř, P. Vibrational Averaging of the Chemical Shift in Crystalline  $\alpha$ -Glycine. *J. Comput. Chem.* **2012**, *33*, 1080-1089.

64. Dračinský, M.; Hodgkinson, P. Effects of Quantum Nuclear Delocalisation on NMR Parameters from Path Integral Molecular Dynamics. *Chem. Eur. J.* **2014**, *20*, 2201-2207.

65. Dračinský, M.; Bouř, P.; Hodgkinson, P. Temperature Dependence of NMR Parameters Calculated from Path Integral Molecular Dynamics Simulations. *J. Chem. Theory Comput.* **2016**, *12*, 968-973.

66. Dovesi, R.; Saunders, V. R.; Roetti, C.; Orlando, R.; Zicovich-Wilson, C. M.; Pascale, F.; Civalleri, B.; Doll, K.; Harrison, N. M.; Bush, I. J.; D'Arco, P.; Llunell, M.; Causà, M.; Noël, Y., *Crystal14 User's Manual*. University of Torino: Torino, 2014.
67. Becke, A. D. Density-Functional Thermochemistry 3. The Role of Exact Exchange. *J. Chem. Phys.* **1993**, *98*, 5648-5652.
68. Lee, C. T.; Yang, W. T.; Parr, R. G. Development of the Colle-Salvetti Correlation-Energy Formula into a Functional of the Electron-Density. *Phys. Rev. B* **1988**, *37*, 785-789.
69. Zhao, Y.; Truhlar, D. G. A New Local Density Functional for Main-Group Thermochemistry, Transition Metal Bonding, Thermochemical Kinetics, and Noncovalent Interactions. *J. Chem. Phys.* **2006**, *125*, 194101-194119.
70. Zhao, Y.; Truhlar, D. G. The M06 Suite of Density Functionals for Main Group Thermochemistry, Thermochemical Kinetics, Noncovalent Interactions, Excited States, and Transition Elements: Two New Functionals and Systematic Testing of Four M06-Class Functionals and 12 Other Functionals. *Theor. Chem. Acc.* **2008**, *120*, 215-241.
71. Dračinský, M.; Hodgkinson, P. A Molecular Dynamics Study of the Effects of Fast Molecular Motions on Solid-State NMR Parameters. *CrystEngComm* **2013**, *15*, 8705-8712.
72. Holmes, S. T.; Iuliucci, R. J.; Mueller, K. T.; Dybowski, C. Semi-Empirical Refinements of Crystal Structures Using  $^{17}\text{O}$  Quadrupolar-Coupling Tensors. *J. Chem. Phys.* **2017**, *146*.
73. Bryce, D. L.; Gee, M.; Wasylishen, R. E. High-Field Chlorine NMR Spectroscopy of Solid Organic Hydrochloride Salts: A Sensitive Probe of Hydrogen Bonding Environment. *J. Phys. Chem. A* **2001**, *105*, 10413-10421.

74. Zamar, R. C.; Gonzalez, C. E.; Pusiol, D. J. Temperature-Induced Orientational Disorder in NaClO<sub>3</sub>. *Phys. Rev. B* **1998**, *58*, 2476-2481.
75. Dračinský, M.; Čechová, L.; Hodgkinson, P.; Procházková, E.; Janeba, Z. Resonance-Assisted Stabilisation of Hydrogen Bonds Probed by NMR Spectroscopy and Path Integral Molecular Dynamics. *Chem. Commun.* **2015**, *51*, 13986-13989.
76. Ghazaryan, V. V.; Fleck, M.; Petrosyan, A. M. New Salts of Amino Acids with Dimeric Cations. *Proc Spie* **2011**, *7998*.
77. Thompson, H. P. G.; Day, G. M. Which Conformations Make Stable Crystal Structures? Mapping Crystalline Molecular Geometries to the Conformational Energy Landscape. *Chem. Sci.* **2014**, *5*, 3173-3182.
78. Nyman, J.; Day, G. M. Static and Lattice Vibrational Energy Differences between Polymorphs. *CrystEngComm* **2015**, *17*, 5154-5165.
79. Harris, R. K.; Hodgkinson, P.; Zorin, V.; Dumez, J. N.; Elena-Herrmann, B.; Emsley, L.; Salager, E.; Stein, R. S. Computation and NMR Crystallography of Terbutaline Sulfate. *Magn. Reson. Chem.* **2010**, *48*, S103-S112.
80. Kibalchenko, M.; Lee, D.; Shao, L. M.; Payne, M. C.; Titman, J. J.; Yates, J. R. Distinguishing Hydrogen Bonding Networks in Alpha-D-Galactose Using NMR Experiments and First Principles Calculations. *Chem. Phys. Lett.* **2010**, *498*, 270-276.
81. Widdifield, C. M.; Robson, H.; Hodgkinson, P. Furosemide's One Little Hydrogen Atom: NMR Crystallography Structure Verification of Powdered Molecular Organics. *Chem. Commun.* **2016**, *52*, 6685-6688.

# TOC Graphic

